Least-squares imaging and deconvolution using the hybrid norm conjugate-direction solver

Yang Zhang and Jon Claerbout

ABSTRACT

To retrieve a sparse model, we applied the hybrid norm conjugate-direction (HBCD) solver proposed by Claerbout to two interesting geophysical problems: least-squares imaging and blind deconvolution. The results showed that this solver is robust for generating sparse models.

INTRODUCTION

L1 norm optimization in many situations are more desirable than the conventional least squares (L2) optimization. However currently widely used methods like IRLS (Iterative Reweighted Least Squares) or weighted-median (Claerbout and Muir, 1973; Darche, 1989; Guitton, 2005) require the users to fine tune extra solver parameters in order to obtain a pleasing result. The sensitivity of such parameters make the solvers cumbersome to use since the users have to do trial-and-error. We developed a robust and efficient L1-type solver (Claerbout, 2009b) that uses a hybrid norm function to approximate the L1 norm, and implemented a generalized conjugate-direction (CD) method by using Taylor's expansion (Maysami and Mussa, 2009).

This solver is convenient to apply, because the function interface is almost the same as the traditional least-squares (L2) solver in the SEP library. The user must specify one additional parameter: the residual quantile. Fortunately this parameter has a clear physical meaning (Claerbout, 2009b). Users should assign this parameter according to prior observation or expectation of the model's spikiness/blockness.

In this paper we show the usefulness of the hybrid solver by applying it on the LSI imaging and deconvolution problems. The $L1$ inversion of LSI imaging (Least Squares Inverse) problem is preferable to L2 inversion, because it better perseves the spikiness/sparseness that are commonly encountered in reflectivity models. When the model regularization is posed with the L2 norm, it is hard to honor spikness/sparseness, because the L2 norm cannot tolerate large values in the model. In contrast, the L1 type norm fits our regularization goal very well.

A similar motivation applies to the deconvolution problem; conventional deconvolution assumes the reflectivity series to be random (white spectrum), whereas we argue that a sparse reflectivity series is more appropriate (and often more desirable) in practice.

APPLICATION – LEAST-SQUARES INVERSE IMAGING

This application originated from the work of target-oriented wave-equation LSI imaging, as described in M. Clapp and Biondi (2005); Valenciano (2006); Tang (2008). The concept of LSI imaging starts with a simple inversion problem:

$$\mathbf{F(m)} = ||\mathbf{Lm} - \mathbf{d_{obs}}||_\mathbf{2}, \tag{1}$$

where $\mathbf{L}$ is a linearized wave-equation modeling operator, the adjoint of which is the imaging operator, $\mathbf{m}$ is the subsurface *reflectivity* model, and $\mathbf{d_{obs}}$ is the observed surface seismic data. In theory, the solution to this inversion problem can be written as follows:

$$\mathbf{m} = \mathbf{H}^+\mathbf{L}'\mathbf{d}_{\text{obs}}, \tag{2}$$

Where $\mathbf{H} = \mathbf{L}'\mathbf{L}$ is called Hessian operator, and $\mathbf{H}^+$ is the pseudo inverse of $\mathbf{H}$. In practice, it is usually impossible to invert $\mathbf{H}$ directly; thus a gradient-based optimization method is often used to find the solution.

One disadvantage of this data-space inversion scheme is that it can not be computed in a target-oriented way, since theoretically even a local perturbation in the model space will affect the entire data space and vice versa. To overcome this difficulty, Valenciano (2006) transformed (1) to a model space inversion based on (2):

$$\mathbf{J(m)} = ||\mathbf{Hm} - \mathbf{L}'\mathbf{d}_{obs}||_2.$$

Valenciano (2008) and Tang (2008) showed that unlike $\mathbf{L}$, matrix $\mathbf{H}$ is usually very sparse (i.e., most of the non-zero elements are centered around the diagonal); thus despite the huge size of $\mathbf{H}$, it is feasible to store an approximation of $\mathbf{H}$ matrix by keeping only a few off-diagonal elements without losing much accuracy.

If we write $\mathbf{m}_{mig} = \mathbf{L}'\mathbf{d}_{obs}$, and add a model regularization term (since most likely $\mathbf{H}$ has a null space). Then the inversion formula is

$$\boldsymbol{J}(\mathbf{m}) = ||\boldsymbol{H}\mathbf{m} - \mathbf{m}_{mig}||_2 + \epsilon||\mathbf{m}||_{norm},$$

in which we applied the hybrid norm to the regularization term.

Tang (2009) provided a way to efficiently compute the Hessian matrix using the phase-encoding technique, and this Hessian matrix is computed only once and stored for all iterations.

Numerical example

The reflectivity model we started with is a cropped subsalt region from the sigsbee2A reflectivity model, as shown in Figure 1(a). Notice that it is quite sparse.

Figure 1(b) shows the input migrated image $\mathbf{m_{mig}}$. While the data $\mathbf{d}$ is modeled with a two-way wave equation, both the migrated image $\mathbf{m_{mig}} = \mathbf{L}'\mathbf{d}$ and the Hessian

operator are computed using a one-way wave-equation propagator. Therefore the data contains non-linear information (e.g., multiples) that cannot be resolved by the linearized one-way wave-equation operator. This explains some of the migration artifacts in the migrated image.

The explicit Hessian operator is computed using the receiver-side random-phase encoding method (Tang, 2008). The size of off-diagonal elements at each image point is 21×21. After the Hessian is computed, we extract the portion corrsponds to the above reflectivity model.

Figure 2(a) and 2(b) shows the inversion result of L2 and hybrid . The first thing to notice is that neither method can perfectly retrieve the original model; nonetheless, there is a significant improvement in the L1 inversion. The sharp boundary of the reflectors at the left of the image is better recovered in the hybrid result.

Figure 2(c) and 2(d) shows the data fitting errors of the two inversion are plotted. By evaluating the total energy of the fitting error (3.48% for both inversion results, $p_e = ||\mathbf{Hm} - \mathbf{m_{mig}}||_\mathbf{2}/||\mathbf{m_{mig}}||_\mathbf{2}$), we claim that hybrid inversion and L2 inversion fit the data almost equally well. This ensures that the major effect of the regularization is to fill the null space of $\mathbf{H}$, with little effect on the data-fitting. However it is true that the data fitting residual of hybrid inversion appears to be more correlated to the reflectivity model than that of L2 inversion is.

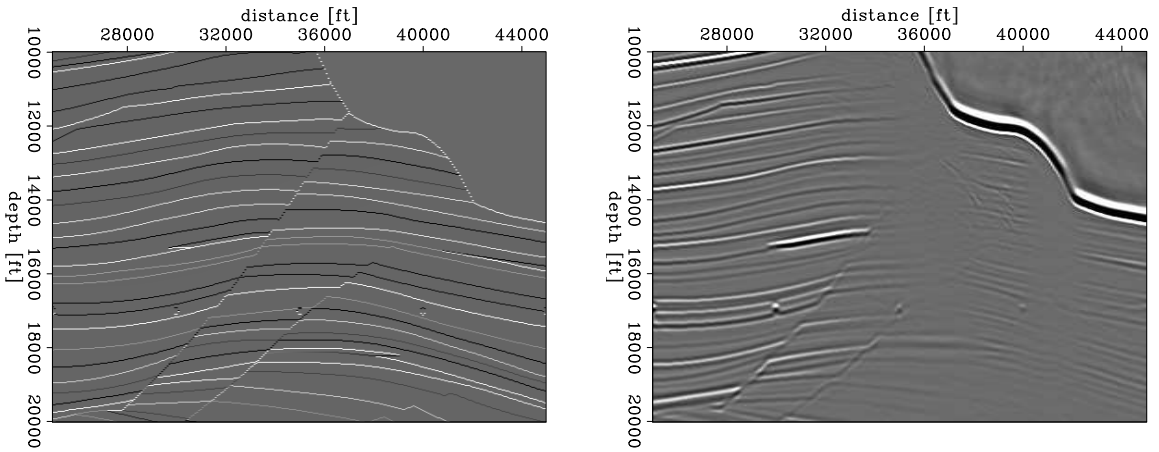

Figure 1: (a) Reflectivity model; (b) input migrated image. [**ER**]

In addition, notice that some parts of the sub-salt reflectors presented in the L2 result are missing in the hybrid result. The reason is clear: the hybrid norm is less tolerant of small values in the residual and always tries to put them down to zero (Claerbout, 2009b). This example shows that this feature of the hybrid norm is not always desirable.

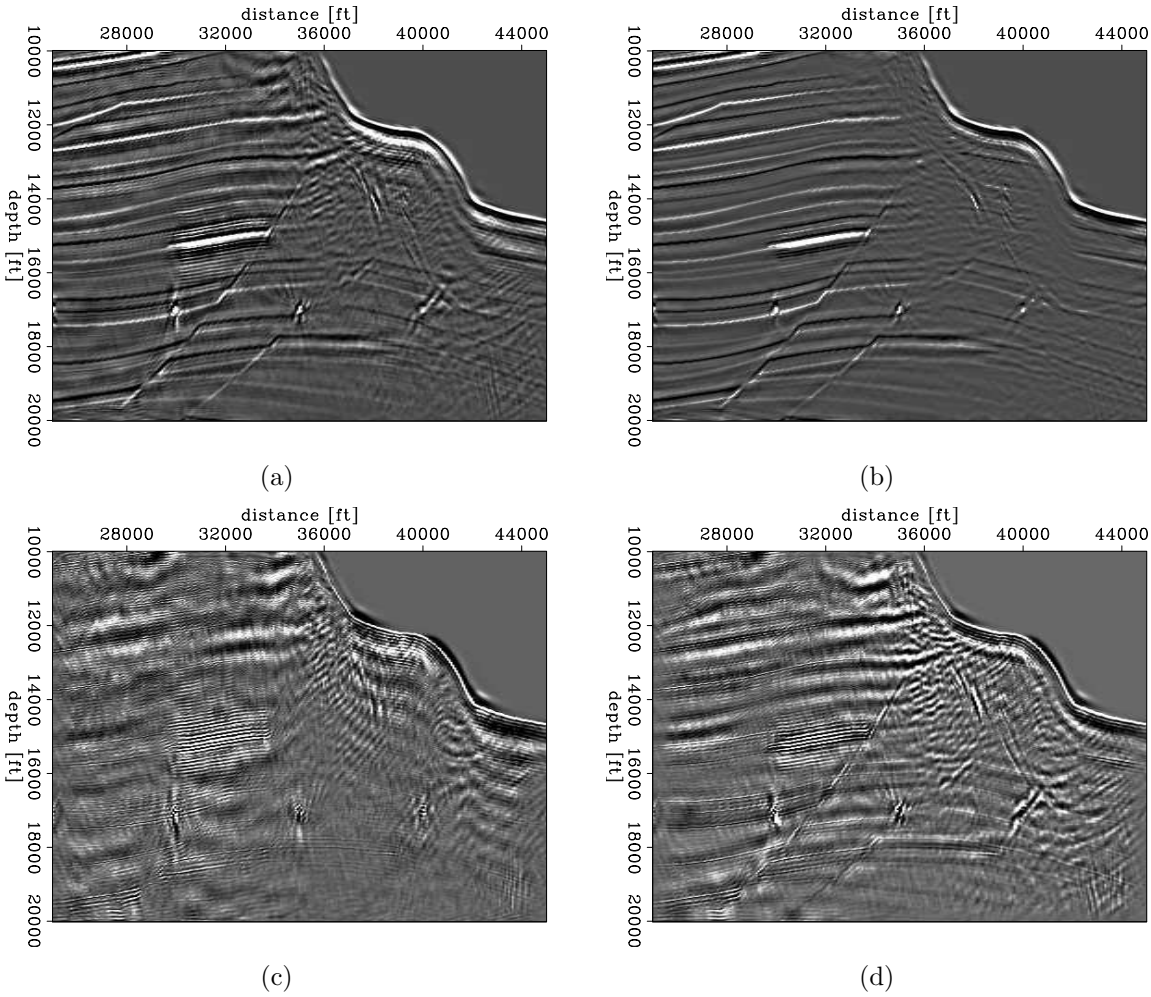

Figure 2: Comparison of the inversion results with L2 and hybrid regularization. (a): L2 inversion result; (b): hybrid inversion result; (c): L2 data fitting residual (d): hybrid data fitting residual. [**ER**]

APPLICATION – DECONVOLUTION

Deconvolution has been a well-known geophysical problem since the 1950s. We investigate the spiking deconvolution, which aims to compress the source wavelet, such that a reflectivity series with higher resolution can be obtained. The simple convolution model is expressed as follows:

$$m(t) * s(t) + n(t) = d(t) \tag{3}$$

where r(t) is the reflectivity series, s(t) is the source wavelet, n(t) is random noise, and d(t) is the seismic traces (we assume a certain kind of amplitude compensation has already been applied).

Intrinsically, this is an under-determined problem, because both $r(t)$ and $s(t)$ are unknown. Further assumptions about the reflectivity series are needed in order to get a deterministic answer. In the L2 scenario, the underlying assumption is that the reflectivity model is purely random (i.e., has a *white spectrum*). As mentioned before, the model may in fact be spiky, which is better matched by an L1 type inversion. Therefore the hybrid result should outperform the L2 result.

For simplicity, we also assume that source wavelet is minimum phased. The conventional spiking deconvolution can be defined as an inverse problem,

$$\mathbf{Da} \approx \mathbf{0},$$

where $\mathbf{D}$ is the data convolution operator, and $\mathbf{a}$ is the filter. In this formulation, the filter is the only unknown, and in theory the data residual itself is the reflectivity model.

To incorporate the model regularization into the inversion framework, we generalize the formulation above by posing the deconvolution problem as such inversion problem:

$$\left\{ \begin{bmatrix} \mathbf{D} & -\mathbf{I} \\ \mathbf{0} & \epsilon\mathbf{I} \end{bmatrix} \begin{bmatrix} \mathbf{a} \\ \mathbf{m} \end{bmatrix} \approx \begin{bmatrix} \mathbf{0} \\ \mathbf{0} \end{bmatrix}, \right. \tag{4}$$

in which $\mathbf{D}$ is the data convolution operator, $\mathbf{a}$ is the filter, and $\mathbf{m}$ is the reflectivity model. The parameter ϵ indicates the strength of the regularization. Since the source wavelet is assumed to be a minimum-phase wavelet, ideally the inversion gives the exact inverse of the source wavelet to $\mathbf{a}$.

The first equation in (4) (data fitting) implies that after convolving the data with the filter, we should get the reflectivity model; any values that cannot fit the reflectivity model are considered as noise in data. The second equation in (4) is the spiky regularization of the model; thus we apply the hybrid norm.

Deconvolution of synthetic data

We started from a simple synthetic reflectivity model from Basic Earth Imaging by Claerbout (2009a). Figure 3 shows the starting reflectivity model, which is quite

sparse. Figure 4(a) shows the minimum-phase wavelet we designed. Figure 4(b) shows the data generated by convolving the reflectivity model with the wavelet. Convolution is done trace by trace.

Figure 5 compares the result of L2 inversion and L1 inversion (using the hybrid norm). As expected, the conventional L2 result gives a fuzzy model poorly correlated to the original one. In contrast, the hybrid result recovers the original model quite well. For verification, the data residuals are plotted at the bottom of Figure 5; the hybrid result has a fitting error of 0.6%, indicating that the data fitting goal is well honored.

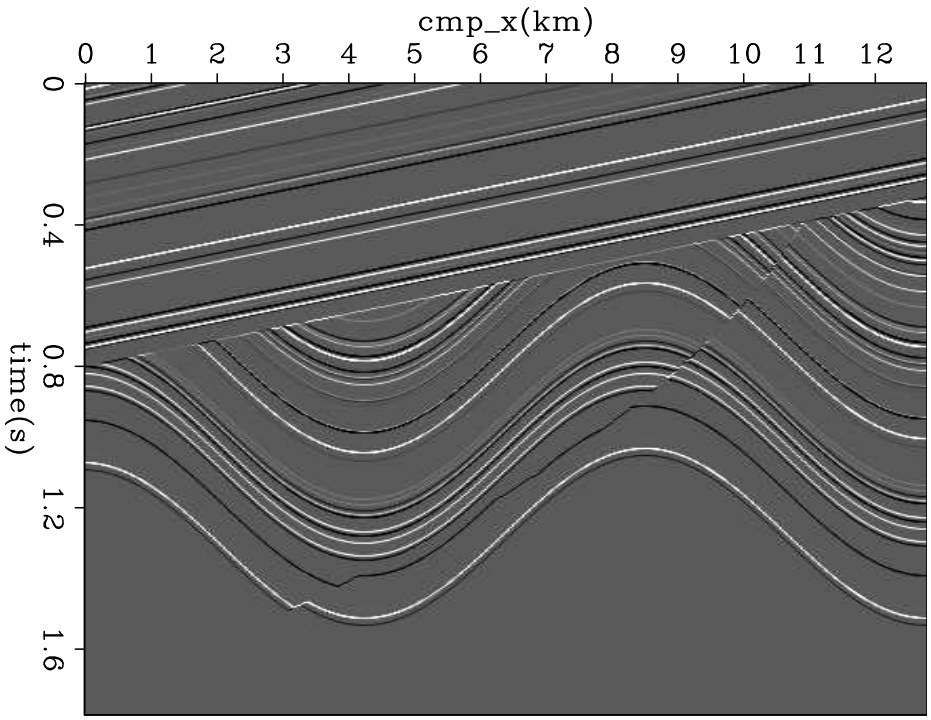

Figure 3: Reflectivity model. [**ER**]

One limitation of the formulation (4) is the assumption of a minimum phase wavelet. A non-minimum phase signal does not have a causal inverse in theory, thus breaking our formulation (4) since the filter **a** that is supposed to be the inverse of source wavelet does not exist.

To see how much the non-minimum phase wavelet will affect the inversion result, we performed another experiment in which the wavelet is chosen to be a non-minimum phase one. Figure 6 shows the new wavelet and the synthetic data generated using this wavelet. Figure 7 shows the result of L2 inversion and L1 inversion (using the hybrid norm) of this data, using the same parameters as in the previous synthetic example. In contrast to the significant improvement obtained before, the hybrid result cannot yield a sparse model because it is impossible to find a filter **a** that undoes the source wavelet.

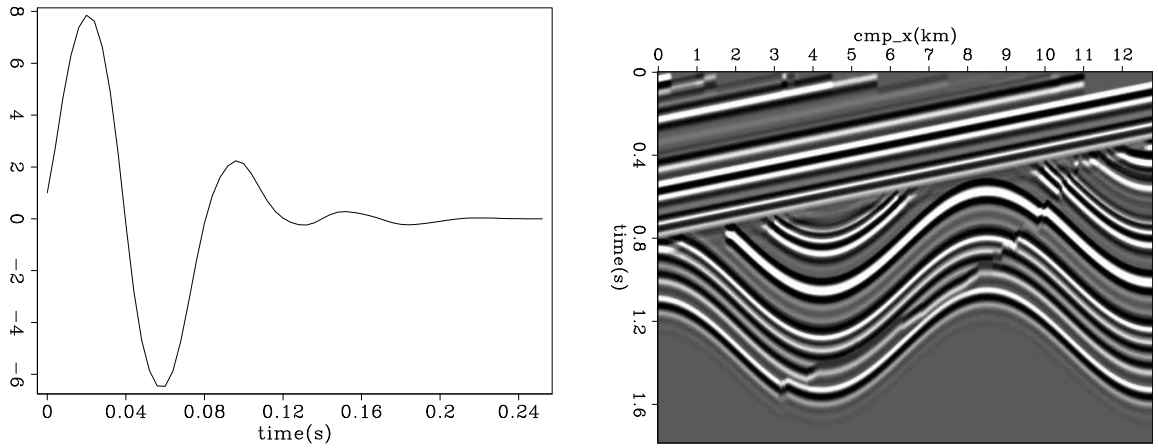

(a) (b)

Figure 4: Synthetic Data for deconvolution. (a): The minimum phase wavelet; (b): generated input data. [**ER**]

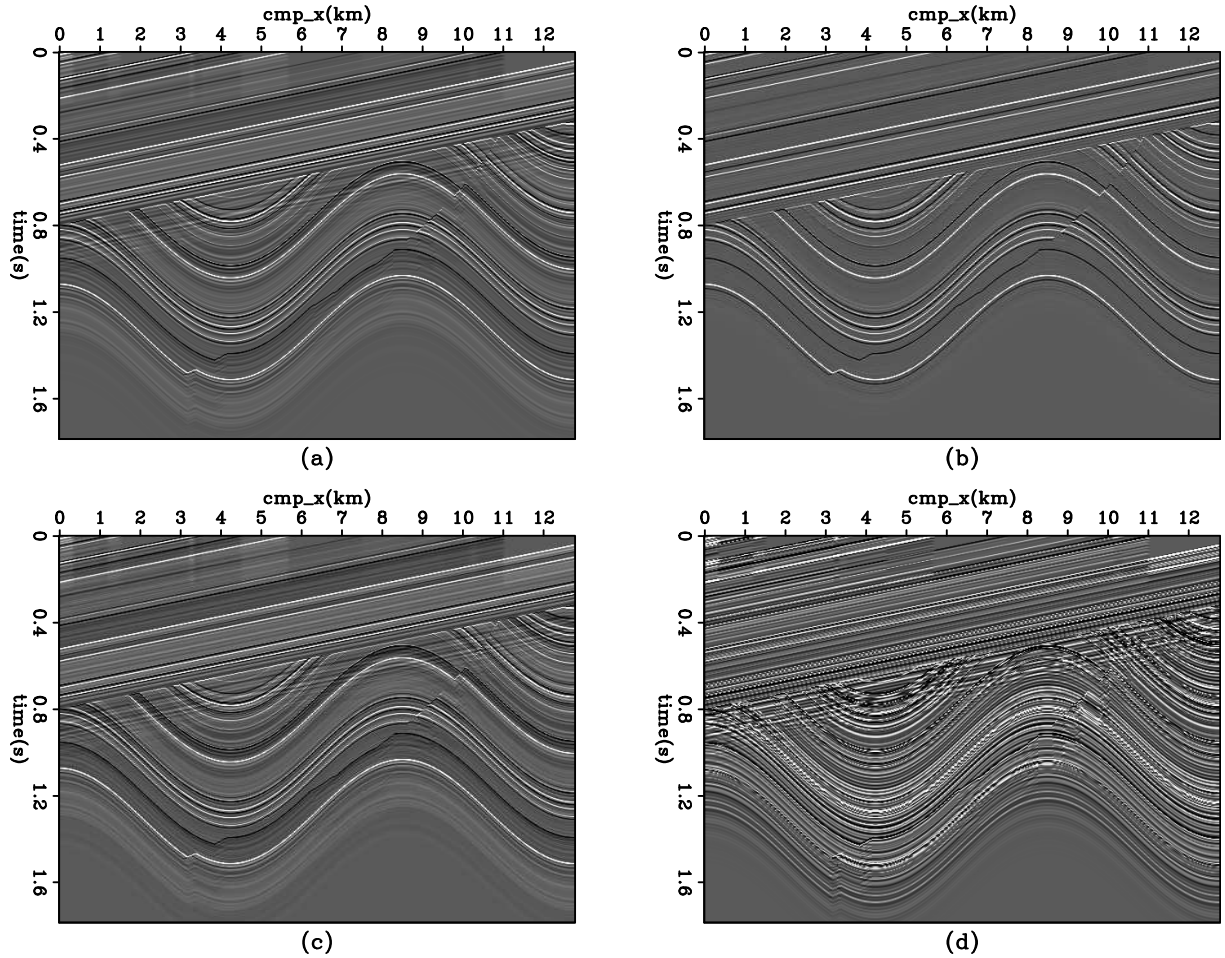

Figure 5: Comparison of deconvolution result for synthetic data. Top panels show the reflectivity model obtained by L2 inversion (a) and hybrid inversion (b); bottom panels (c)(d) show the respective data residual. [**ER**]

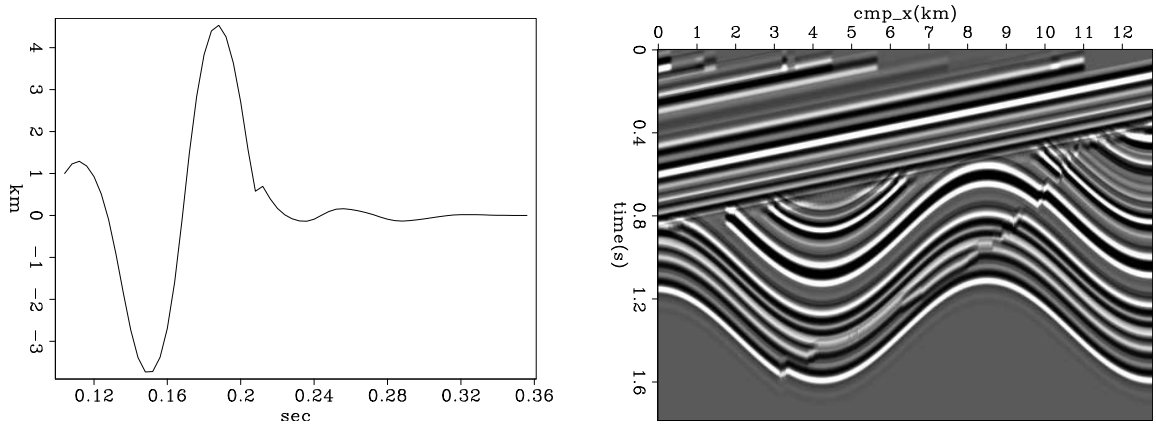

(a) (b)

Figure 6: (a): the mixed-phase wavelet; (b): generated data. [**ER**]

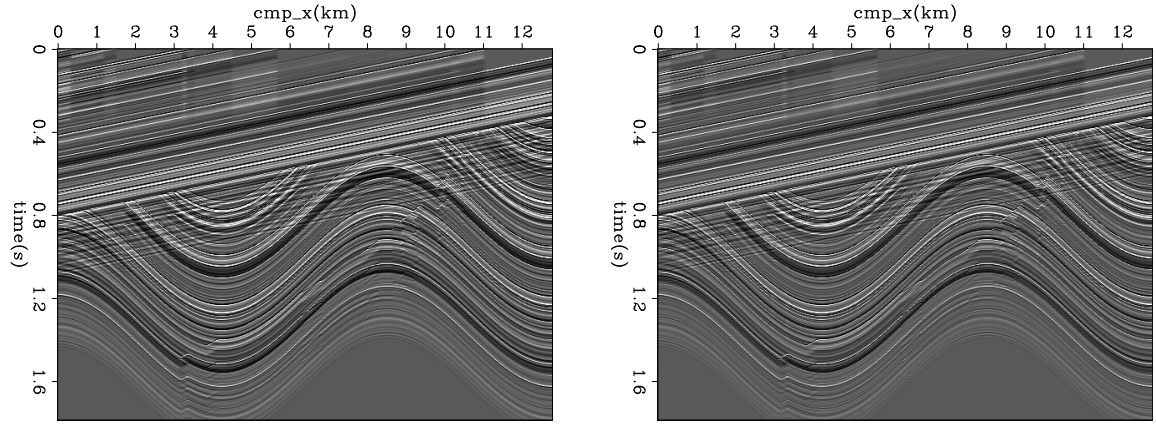

(a) (b)

Figure 7: (a): L2 inversion result for the synthetic data generated with mixed-phase wavelet;(b): hybrid inversion result. [**ER**]

Deconvolution of a common-offset field data

The second example is a common-offset section of field marine data. Figure 8 shows the input data.

Figure 9 shows the deconvolution result using L2 and L1 inversion. Although in this case the L1 inversion gives a cleaner model, the model is less desirable. Some areas of interest (like the salt-bottom) are suppressed by regularization due to lower amplitude than do the salt-top and sea-bed. In other words, the regularization is too strong. The bottom panel of Figure 9 showing the data fitting residual further confirms this point. From the amplitude information of this plot, roughtly 20% of

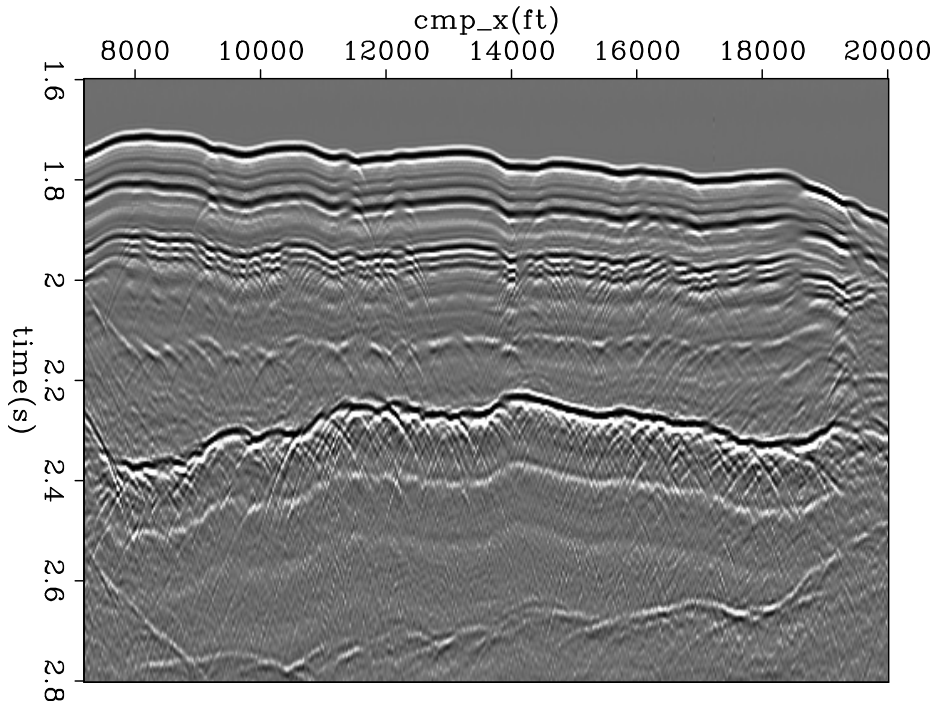

Figure 8: Input Common Offset data. [**ER**]

the data was pushed into fitting error, the regularization distorts the data fitting too much rather than eliminating the model's null space.

Our predicament in this case is that if we set ϵ to a small value, then the hybrid result does not differ significantly from L2 result; on the other hand a large ϵ is not desirable either. Something in the data breaks our simple deconvolution model.

Figure 10 shows one trace extracted from the section. Thanks to the sparseness of the reflector, it is easy to identify the waveforms of several strong reflections. Take the very first sea bed reflection for instance, the wavelet is quite symmetric, more likely zero phase instead of minimum phase. From the lesson we have learned from the synthetic data, it is likely that the non minimum phase wavelet causes the failure of the method (4).

Fortunately, it is easy to identify the wavelets at several strong reflections, so we can roughly extract the wavelet from these locations and use this wavelet in the convolution model. The simplified inversion problem can be defined as follows:

$$\left\{ \begin{array}{rcl} \mathbf{Sm} & \approx & \mathbf{d} \\ \epsilon\mathbf{m} & \approx & \mathbf{0} \end{array} \right. \tag{5}$$

in which $\mathbf{S}$ is the convolution operator of the known wavelet $\mathbf{s}$, $\mathbf{m}$ is the unknown model, and $\mathbf{d}$ is the seismic data.

Figure 11 shows the extracted source wavelet by averaging the wavelet at the sea-

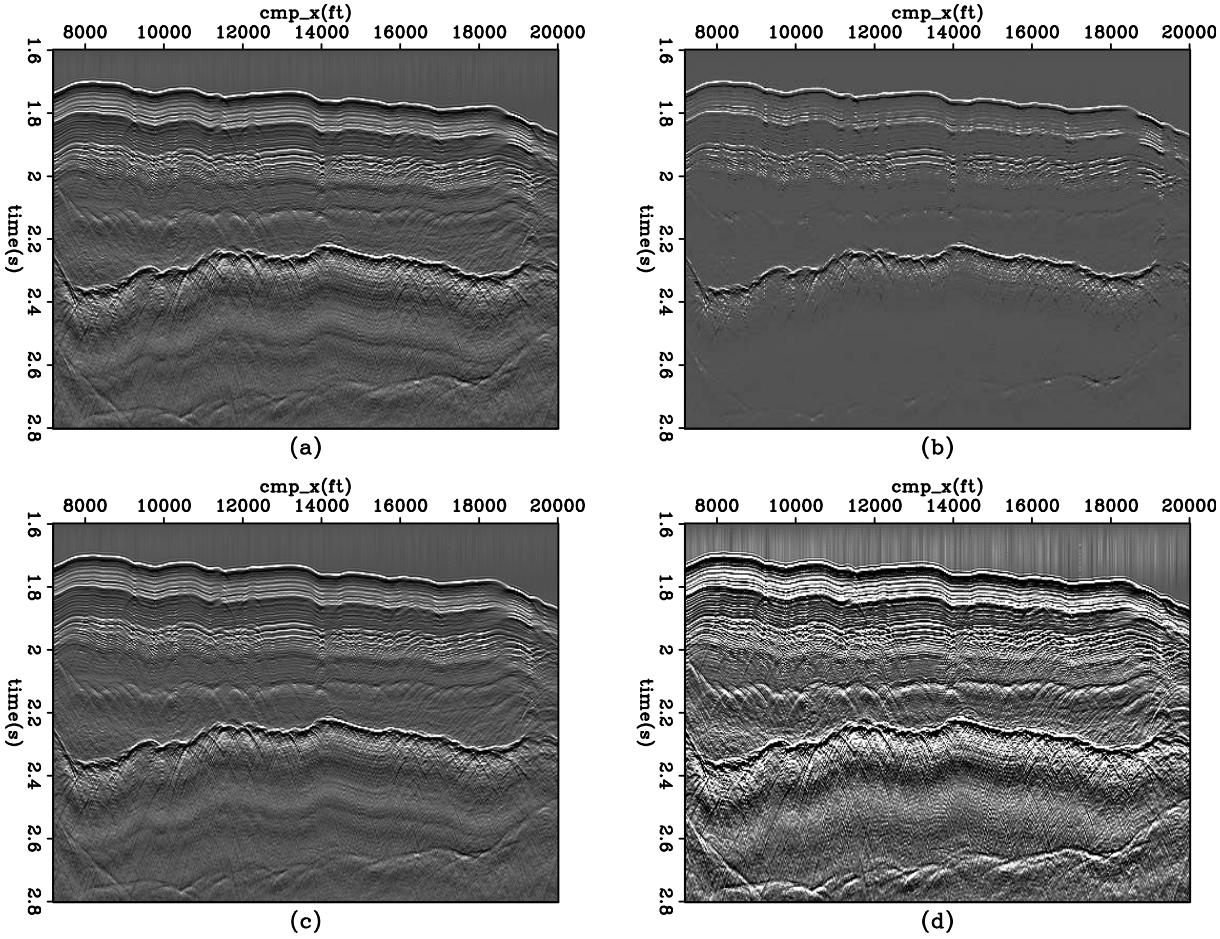

Figure 9: Top: L2 (a) and hybrid (b) deconvolution result for the Common Offset data; bottom: data fitting residuals of L2 (c) and hybrid (d) inversion. [**ER**]

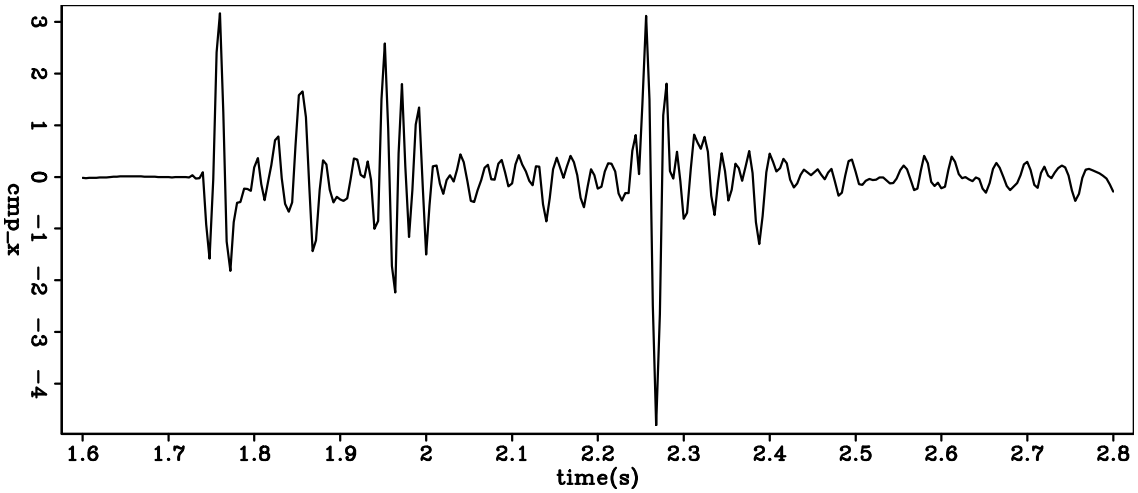

Figure 10: One single trace extracted at 12000m of the common offset section. [**ER**]

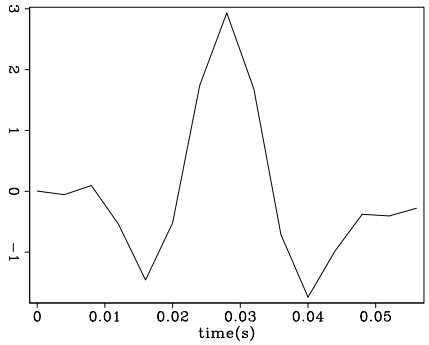

Figure 11: The extracted source wavelet from seismic data. [**CR**]

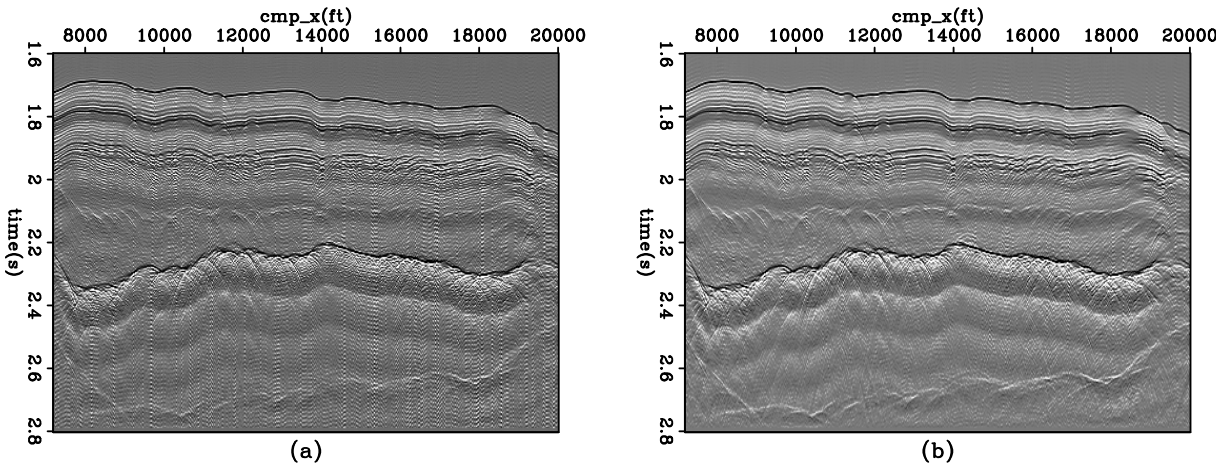

Figure 12: (a): the L2 inversion result; (b) the hybrid inversion result. [**ER**]

floor reflection among all traces. Figure 12 shows the result of L2 inversion and hybrid inversion. Compared with the orginal data, both deconvolution results improve the spatial resolution; and the hybrid result is less noisy than the L2 result.

Discussion

It is not always true that wavelet can be extracted from the seismic data, in this case we have to perform *blind* deconvolution. To overcome the difficulty brought by non-minimum phase wavelet, we turn back to the original non-linear convolution model (3), and solve the non-linear inversion problem directly.

There are two ways to linearize this model. The first one is to use model perturbation and neglect the non-linear higher order terms in the following:

$$(\mathbf{s}+\mathbf{\Delta s})*(\mathbf{m}+\mathbf{\Delta m})\approx \mathbf{s}*\mathbf{m}+\mathbf{s}*\mathbf{\Delta m}+\mathbf{m}*\mathbf{\Delta s}=\mathbf{d},$$

in which $\mathbf{m}$, $\mathbf{s}$ are the initial model and source wavelet respectively. $\mathbf{\Delta m}, \mathbf{\Delta s}$ are the pertubation of them, the linearized inversion will output $\mathbf{\Delta m}, \mathbf{\Delta s}$. The other way of linearization is a two-stage linear least squares formulation; i.e. alternately fixing one term ($\mathbf{m}$ or $\mathbf{s}$) and inverting for the other one. First use an initial wavelet $\mathbf{s}$, keep $\mathbf{s}$ unchanged and invert for model $\mathbf{m}$

$$\mathbf{Sm}=\mathbf{d}, \tag{6}$$

and then use the updated $\mathbf{m}$ to invert for wavelet $\mathbf{s}$

$$\mathbf{Ms}=\mathbf{d}. \tag{7}$$

Repeat this process (6) and (7) for several iterations.

As is in all non-linear inversion problems, the difficulty in these methods is to find a good starting model. Another issue is to add proper constrain on the wavelet $\mathbf{s}$, for example, the wavelet should have constant energy during inversion, but this constrain does not fit the linear inversion framework.

CONCLUSION

We demonstrated that by using hybrid solver, it is robust and convinient to generate sparse models in Least-Squares Inverse imaging and deconvolution problems; although in the blind deconvolution formulation the L2 and hybrid inversion would yield similar results in the absence of minimum phase wavelet assumption.

ACKNOWLEDGMENTS

The authors would like to thank the sponsors of Stanford Exploration Project for the financial support, and also thank Bob Clapp, Luis Canales, Ali Almomin and Elita Li for the fruitful discussion.

REFERENCES

Claerbout, J. F., 2009a, Basic earth imaging.

———, 2009b, Blocky models via the l1/l2 hybrid norm: SEP-Report, **139**, 1–10.

Claerbout, J. F. and F. Muir, 1973, Robust modeling with erratic data: Geophysics, **18**, 826–844.

Darche, G., 1989, Iterative l_1 deconvolution: SEP 61, 281–302.

Guitton, A., 2005, Multidimensional seismic noise attenuation: PhD thesis, Stanford University.

M. Clapp, R. C. and B. Biondi, 2005, Regularized least-squares inversion for 3-d subsalt imaging: Soc. of Expl. Geophys., 1814–1817.

Maysami, M. and N. Mussa, 2009, Generalized-norm conjugate direction solver: SEP-Report, **139**, 11–22.

Tang, Y., 2008, Wave-equation hessian by phase encoding: SEP-Report, **134**, 1–25.

———, 2009, Inversion with phase-encoded hessian: Geophysics, **74**, WCA95–WCA107.

Valenciano, A., 2006, Target-oriented wave-equation inversion: Geophysics, **71**, A35–38.

———, 2008, Imaging by wave-equation inversion: PhD thesis, Stanford University.

Chris Leader graduated from Oxford Univeristy in 2008 with a BA in Physics (with concentration on Astrophysics and Condensed Matter physics) and then from Imperial College London in 2009 with an MSc in Petroleum Geophysics (Distinction). He is currently a first year student in the Stanford Exploration Project on the PhD program working on Fourier methods of regularisation. Work experience involves 3D seismic processing for a Rio Tinto acquired dataset over summer 2009. He is a member of SEG, EAGE, PESGB and IOP.

Yunyue (Elita) Li graduated from China University of Petroleum, Beijing in July 2008 with a B.S. in Information and Computational Science. She joined SEP in the fall of 2008, and is currently working toward a Ph.D. in Geophysics. She is a student member of the SEG.

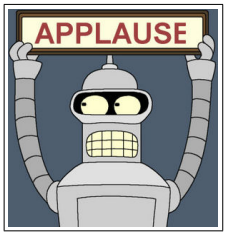

Nader Moussa graduated from North Carolina State University, where he studied Physics and Electrical and Computer Engineering. In 2008, he finished his M.Sc. at Stanford in Electrical Engineering, with focus on experimental radioscience and electromagnetic sensor instrumentation design. He is now working towards a Ph.D. in Geophysics with the Stanford Exploration Project.